Figure 3. ECHS1 expression and enzyme activity. ECHS1 expression was analyzed by immunoblotting. C1/2, control; P, patient. Mitochondrial fraction prepared from patient's skeletal muscle (**A**) or whole-cell lysate (**B**) and mitochondrial fraction (**C**) prepared from the patient-derived myoblasts were analyzed via immunoblotting. All findings indicated that ECHS1 levels in patient samples were too low to detect by immunoblotting. **D**: RT-PCR was used to assess *ECHS1* mRNA levels in the patient. Notably, patient-derived myoblasts and control myoblasts did not differ with regard to *ECHS1* mRNA level. **E**: Mitochondrial fractions prepared from patient-derived myoblasts were used to estimate ECHS1 enzyme activity in the patient. All ECHS1 activity measurements were normalized to CS activity; ECHS1 activity in patient-derived samples was 13% of that in control samples. The experiments were performed in triplicate. Error bars represent standard deviations. (** $P < 0.005$ Student's t-test).
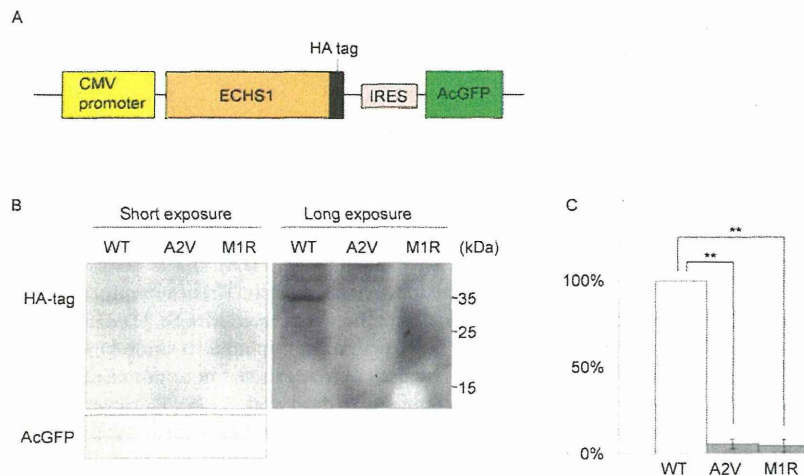

Figure 4. Exogenous expression of mutant ECHS1 protein in cancer cells. **A**: Schematic diagram of the pIRES mammalian expression vector. **B**: Representative image of an immunoblotting containing AcGFP, an internal control, and each HA-tagged ECHS1 protein; all proteins were isolated from DLD-1 cells that transiently overexpressed wild-type, A2V, or M1R HA-tagged ECHS1 from pIRES. The images obtained by short exposure (left) and long exposure (right). **C**: Overexpressed HA-tagged ECHS1 protein levels. Both mutant ECHS1 proteins showed dramatically decreased expression compared to wild-type ECHS1 protein, when ECHS1 was normalized relative to the internal control. Each experiment was performed in triplicate. Error bars represent standard deviations (** $P < 0.005$ Student's t-test).

Discussion

Here, we described a patient harboring compound heterozygous mutations in *ECHS1*. Immunoblotting analysis revealed that ECHS1 protein was undetectable in patient-derived myoblasts; moreover, these cells showed significantly lower ECHS1 enzyme activity than controls. Exogenous expression of two recombinant mutant proteins in DLD-1 cells showed c.2T>G; p.M1R and c.5C>T; p.A2V mutations affected ECHS1 protein expression. Cellular complementation experiment verified the patient had ECHS1 deficiency.

The c.2T>G; p.M1R mutation affected the start codon and therefore was predicted to impair the protein synthesis from canonical
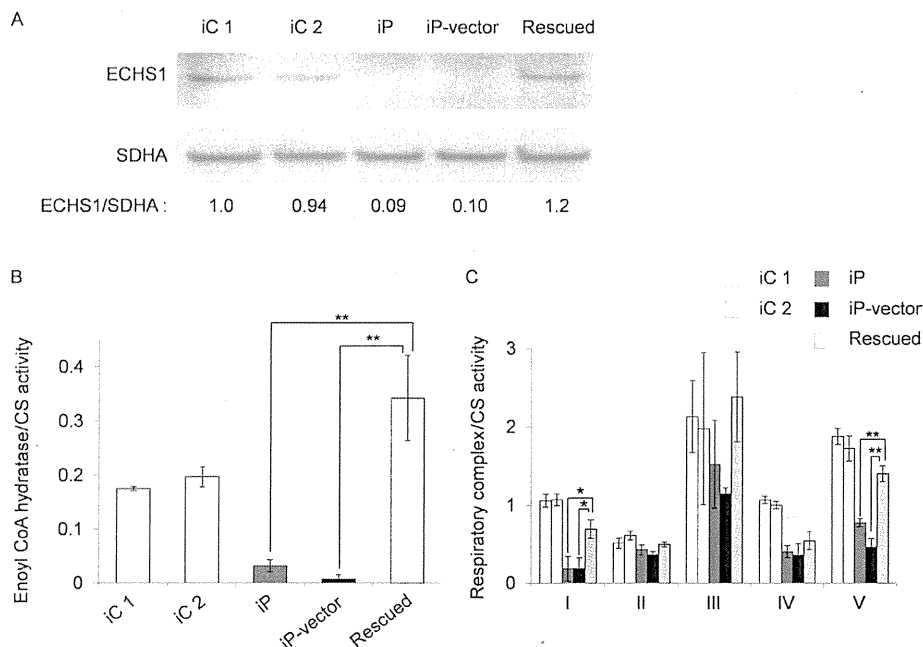
Figure 5. ECHS1 protein expression and enzyme activity in rescued myoblasts. An empty vector or a construct encoding wild-type ECHS1 was introduced into immortalized patient-derived myoblasts. iC1/2, immortalized control myoblasts; iP, immortalized patient-derived myoblasts; iP-vector, immortalized patient-derived myoblasts transfected with empty vector; Rescued, immortalized patient-derived myoblasts stably expressing wild-type ECHS1. **A:** ECHS1 levels were assessed on immunoblotting using mitochondrial fractions prepared from rescued myoblasts. ECHS1 level in "rescued" is 11 times higher than that in "iP-vector". **B:** Mitochondrial fractions prepared from rescued myoblasts were also used to measure ECHS1 enzyme activity. ECHS1 activity normalized to CS activity in "rescued" was 49 times higher than that in "iP-vector." Each experiment was performed in triplicate. Error bars represent standard deviations ($^{**}P < 0.005$ Student's t-test). **C:** Mitochondrial fractions prepared from rescued myoblasts were used to measure enzyme activities of mitochondrial respiratory complexes. Activity values were normalized to CS activity. Activities of complexes I, IV, and V were mostly restored from "iP" and "iP-vector." In "rescued," the enzyme activities of complexes I, IV, and V were 3.5, 1.3, and 2.2 times higher, respectively, than the "iP-vector." Each experiment was performed in triplicate. Error bars represent standard deviations ($^{**}P < 0.005$, $^{*}P < 0.05$ Student's t-test).

initiation site. In the reference *ECHS1* sequence, the next in-frame start codon is located in amino acids 97 (Fig. 2C). Even if translation could occur from this second start codon, the resulting product would lack the whole transit peptide and part of the enoyl-CoA hydratase/isomerase family domain (Fig. 2C). The c.5C>T; p.A2V mutation was located in the mitochondrial transit peptide and the mutation may affect the mitochondrial translocation of ECHS1. Surprisingly, the MitoProt-predicted mitochondrial targeting scores for the wild-type and A2V-mutant proteins were 0.988 and 0.991, respectively [MitoProt II; http://ihg.gsf.de/ihg/mitoprot.html; Claros and Vincens, 1996] and not markedly different from each other. Nevertheless, mislocalized mutant protein may have been degraded outside of the mitochondria. Consistent with this speculation was the finding that immunoblotting of lysate from patient-derived myoblasts (Fig. 3B) or from transfected cells that overexpressed the recombinant p.A2V-mutant ECHS1 (Fig. 4B, Supp. Fig. S2) did not show upper shifted ECHS1 bands that indicated ECHS1 with the transit peptide. Another possible explanation is that the mutation affected the translation efficiency because it was very close to the canonical start codon. It can change secondary structure of ECHS1 mRNA or alter the recognition by the translation initiation factors. As stated above, even if there was a translation product from the second in-frame start codon, that product would probably not function.

This patient presented with symptoms that are indicative of fatty acid oxidation disorders (e.g., hypotonia and metabolic acidosis), but he also presented with neurologic manifestations, including developmental delay and Leigh syndrome, that are not normally associated with fatty acid β-oxidation disorders. Interestingly, developmental delay is also found in cases of SCAD deficiency [Jethva et al., 2008]. In the absence of SCAD, the byproducts of butyryl-CoA—including butyrylcarnitine, butyrylglycine, ethylmalonic acid (EMA), and methylsuccinic acid—accumulate in blood, urine, and cells. These byproducts may cause the neurological pathology associated with SCAD deficiency [Jethva et al., 2008]. EMA significantly inhibits creatine kinase activity in the cerebral cortex of Wistar rats but does not affect levels in skeletal or heart muscle [Corydon et al., 1996]. Elevated levels of butyric acid modulated gene expression because excess butyric acid can enhance histone deacetylase activity [Chen et al., 2003]. Moreover, the highly volatile nature of butyric acid as a free acid may also add to its neurotoxic effects [Jethva et al., 2008].

On the other hand, it is very rare for fatty acid β-oxidation disorders causing Leigh syndrome. Therefore, the most noteworthy manifestation in this patient was Leigh syndrome. Leigh syndrome is a neuropathological entity characterized by symmetrical necrotic lesions along the brainstem, diencephalon, and basal ganglion [Leigh, 1951]. It is caused by abnormalities of mitochondrial energy generation and exhibits considerable clinical and genetic heterogeneity [Chol et al., 2003]. Commonly, defects in the mitochondrial respiratory chain or the pyruvate dehydrogenase complex are responsible for this disease. This patient's skeletal muscle samples exhibited a combined respiratory chain deficiency, and this deficiency may be the reason that he presented with Leigh syndrome. Although it

remained unclear what caused the respiratory chain defect, cellular complementation experiments showed almost complete restoration, indicating there was an unidentified link between ECHS1 and respiratory chain. One of the possible causes of respiratory chain defect is the secondary effect of accumulation of toxic metabolites. For example, an elevated urine glyoxylate was observed in this patient. Although the mechanism of this abnormal accumulation is not clear at the moment, it was shown that glyoxylate inhibited oxidative phosphorylation or pyruvate dehydrogenase complex by in vitro systems [Whitehouse et al., 1974; Lucas and Pons, 1975]. Therefore, we speculate that in our patient, ECHS1 deficiency induced metabolism abnormality including glyoxylate accumulation, and glyoxylate played a role in decreased enzyme activities of respiratory chain complexes. Interestingly, a recent paper describing patients with Leigh syndrome and ECHS1 deficiency showed decreased activity of pyruvate dehydrogenase complex in fibroblasts [Peters et al., 2014], (Supp. Table S5). BN-PAGE showed the assembly of respiratory complex components in the patient was not clearly different from the control (Supp. Fig. S1). This result suggests that the respiratory chain defect in the patient is more likely because of the secondary effect of accumulation of toxic metabolites. On the other hand, many findings indicate interplays between mitochondrial fatty acid β-oxidation and the respiratory chain. For example, Enns et al. [2000] mentioned the possibility of the physical association between these two energy-generating pathways from overlapping clinical phenotypes in genetic deficiency states. More recently, Wang and his colleagues actually showed physical association between mitochondrial fatty acid β-oxidation enzymes and respiratory chain complexes (Wang et al., 2010). Similarly, Narayan et al. demonstrated interactions between short-chain 3-hydroxyacyl-CoA dehydrogenase (SCHAD) and several components of the respiratory chain complexes including the catalytic subunits of complexes I, II, III, and IV via pull-down assays involving several mouse tissues. Considering the role of SCHAD as a NADH-generating enzyme, this interaction was suggested to demonstrate the logical physical association with the regeneration of NAD through the respiratory chain [Narayan et al., 2012]. Still more recently, mitochondrial protein acetylation was found to be driven by acetyl-CoA produced from mitochondrial fatty acid β-oxidation [Pougovkina et al., 2014]. Because the activities of respiratory chain enzymes are regulated by protein acetylation [Zhang et al., 2012], this finding indicated that β-oxidation regulates the mitochondrial respiratory chain. Remarkably, acyl-CoA dehydrogenase 9 (ACAD9), which participates in the oxidation of unsaturated fatty acid, was recently identified as a factor involved in complex I biogenesis [Haack et al., 2010; Heide et al., 2012]. Cellular complementation experiments that involve overexpression of wild-type ACAD9 in patient-derived fibroblast cell lines showed restoration of complex I assembly and activity [Haack et al., 2010]. Accumulating evidence indicates that there are complex regulatory interactions between mitochondrial fatty acid β-oxidation and the respiratory chain.

ECHS1 has been shown to interact with several molecules outside the mitochondrial fatty acid β-oxidation pathway [Chang et al., 2013; Xiao et al., 2013] and the loss of this interaction can affect respiratory chain function in a patient. Further functional analysis of ECHS1 will advance our understanding of the complex regulation of mitochondrial metabolism.

References

Chang Y, Wang SX, Wang YB, Zhou J, Li WH, Wang N, Fang DF, Li HY, Li AL, Zhang XM, Zhang WN. 2013. ECHS1 interacts with STAT3 and negatively regulates STAT3 signaling. FEBS Lett 587:607–613.

Chen JS, Faller DV, Spanjaard RA. 2003. Short-chain fatty acid inhibitors of histone deacetylases: promising anticancer therapeutics? Curr Cancer Drug Targets 3:219–236.

Chol M, Lebon S, Bénit P, Chretien D, de Lonlay P, Goldenberg A, Odent S, Hertz-Pannier L, Vincent-Delorme C, Cormier-Daire V, Rustin P, Rötig A, et al. 2003. The mitochondrial DNA G13513A MELAS mutation in the NADH dehydrogenase 5 gene is a frequent cause of Leigh-like syndrome with isolated complex I deficiency. J Med Genet 40:188–191.

Claros MG, Vincens P. 1996. Computational method to predict mitochondrially imported proteins and their targeting sequences. Eur J Biochem 241:779–786.

Corydon MJ, Gregersen N, Lehnert W, Ribes A, Rinaldo P, Kmoch S, Christensen E, Kristensen TJ, Andresen BS, Bross P, Winter V, Martinez G, et al. 1996. Ethylmalonic aciduria is associated with an amino acid variant of short chain acyl-coenzyme A dehydrogenase. Pediatr Res 39:1059–1066.

Enns GM, Bennett MJ, Hoppel CL, Goodman SI, Weisiger K, Ohnstad C, Golabi M, Packman S. 2000. Mitochondrial respiratory chain complex I deficiency with clinical and biochemical features of long-chain 3-hydroxyacyl-coenzyme A dehydrogenase deficiency. J Pediatr 136:251–254.

Ensenauer R, He M, Willard JM, Goetzman ES, Corydon TJ, Vandahl BB, Mohsen A-W, Isaya G, Vockley J. 2005. Human acyl-CoA dehydrogenase-9 plays a novel role in the mitochondrial beta-oxidation of unsaturated fatty acids. J Biol Chem 280:32309–32016.

Frezza C, Cipolat S, Scorrano L. 2007. Organelle isolation: functional mitochondria from mouse liver, muscle and cultured fibroblasts. Nat Protoc 2:287–295.

Haack TB, Danhauser K, Haberberger B, Hoser J, Strecker V, Boehm D, Uziel G, Lamantea E, Invernizzi F, Poulton J, Rolinski B, Iuso A, et al. 2010. Exome sequencing identifies ACAD9 mutations as a cause of complex I deficiency. Nat Genet 42:1131–1134.

Heide H, Bleier L, Steger M, Ackermann J, Dröse S, Schwamb B, Zörnig M, Reichert AS, Koch I, Wittig I, Brandt U. 2012. Complexome profiling identifies TMEM126B as a component of the mitochondrial complex I assembly complex. Cell Metab 6:538–549.

Hochstrasser DF, Frutiger S, Paquet N, Bairoch A, Ravier F, Pasquali C, Sanchez JC, Tissot JD, Bjellqvist B, Vargas R, Ron DA, Graham JH. 1992. Human liver protein map: a reference database established by microsequencing and gel comparison. Electrophoresis 13:992–1001.

Ikeda Y, Dabrowski C, Tanaka K. 1983. Separation and properties of five distinct acyl-CoA dehydrogenases from rat liver mitochondria. J Biol Chem 258:1066–1076.

Ikeda Y, Hine DG, Okamura-Ikeda K, Tanaka K. 1985a. Mechanism of action of short-chain, medium chain and long-chain acyl-CoA dehydrogenases: direct evidence for carbanion formation as an intermediate step using enzyme-catalyzed C-2 proton/deuteron exchange in the absence of C-3 exchange. J Biol Chem 260:1326–1337.

Ikeda Y, Okamura-Ikeda K, Tanaka K. 1985b. Spectroscopic analysis of the interaction of rat liver short chain, medium chain and long chain acyl-CoA dehydrogenases with acyl-CoA substrates. Biochemistry 24:7192–7199.

Jethva R, Bennett MJ, Vockley J. 2008. Short-chain acyl-coenzyme A dehydrogenase deficiency. Mol Genet Metab 95:195–200.

Kamijo T, Aoyama T, Miyazaki J, Hashimoto T. 1993. Molecular cloning of the cDNAs for the subunits of rat mitochondrial fatty acid beta-oxidation multienzyme complex. Structural and functional relationships to other mitochondrial and peroxisomal beta-oxidation enzymes. J Biol Chem 268:26452–26460.

Kim DW, Uetsuki T, Kaziro Y, Yamaguchi N, Sugano S. 1990. Use of the human elongation factor 1 alpha promoter as a versatile and efficient expression system. Gene 91:217–223.

Kompare M, Rizzo WB. 2008. Mitochondrial fatty-acid oxidation disorders. Semin Pediatr Neurol 15:140–149.

Leigh D. 1951. Subacute necrotizing encephalomyelopathy in an infant. J Neurol Neurosurg Psychiatr 14:216–221.

Lucas M, Pons AM. 1975. Influence of glyoxylic acid on properties of isolated mitochondria. Biochimie 57:637–645.

Matsunaga T, Kumanomido H, Shiroma M, Goto Y, Usami S. 2005. Audiological features and mitochondrial DNA sequence in a large family carrying mitochondrial A1555G mutation without use of aminoglycoside. Ann Otol Rhinol Laryngol 114:153–160.

Morava E, Rodenburg RJ, Hol F, de Vries M, Janssen A, van den Heuvel L, Nijtmans L, Smeitink J. 2006. Clinical and biochemical characteristics in patients with a high mutant load of the mitochondrial T8993G/C mutations. Am J Med Genet A 140:863–868.

Narayan, SB, Master SR, Sirec AN, Bierl C, Stanley PE, Li C, Stanley CA, Bennett MJ. 2012. Short-chain 3-hydroxyacyl-coenzyme A dehydrogenase associates with a protein super-complex integrating multiple metabolic pathways. PLoS One 7: e35048.

Peters H, Buck N, Wanders R, Ruiter J, Waterham H, Koster J, Yaplito-Lee J, Ferdinandusse S, Pitt J. 2014. ECHS1 mutations in Leigh disease: a new inborn error of metabolism affecting valine metabolism. Brain 137: 2903–2908.

Pougovkina O, Te Brinke H, Ofman R, van Cruchten AG, Kulik W, Wanders RJ, Houten SM, de Boer VC. 2014. Mitochondrial protein acetylation is driven by acetyl-CoA from fatty acid oxidation. Hum Mol Genet 23:3513–3522.

Shimazaki H, Takiyama Y, Ishiura H, Sakai C, Matsushima Y, Hatakeyama H, Honda J, Sakoe K, Naoi T, Namekawa M, Fukuda Y, Takahashi Y, et al. 2012. A homozygous mutation of C12orf65 causes spastic paraplegia with optic atrophy and neuropathy (SPG55). J Med Genet 49:777–784.

Spiekerkoetter U, Khuchua Z, Yue Z, Bennett MJ, Strauss AW. 2004. General mitochondrial trifunctional protein (TFP) deficiency as a result of either alpha- or beta-subunit mutations exhibits similar phenotypes because mutations in either subunit alter TFP complex expression and subunit turnover. Pediatr Res 55:190–196.

Steinman HM, Hill RL. 1975. Bovine liver crotonase (enoyl coenzyme A hydratase). Methods Enzymol 35:136–151.

Uchida Y, Izai K, Orii T, Hashimoto T. 1992. Novel fatty acid beta-oxidation enzymes in rat liver mitochondria. II. Purification and properties of enoyl-coenzyme A (CoA) hydratase/3-hydroxyacyl-CoA dehydrogenase/3-ketoacyl-CoA thiolase trifunctional protein. J Biol Chem 267:1034–1041.

Wang Y, Mohsen AW, Mihalik SJ, Goetzman ES, Vockley J. 2010. Evidence for physical association of mitochondrial fatty acid oxidation and oxidative phosphorylation complexes. J Biol Chem 285:29834–29841.

Whitehouse S, Cooper RH, Randle PJ. 1974. Mechanism of activation of pyruvate dehydrogenase by dichloroacetate and other halogenated carboxylic acids. Biochem J 141:761–774.

Xiao CX, Yang XN, Huang QW, Zhang YQ, Lin BY, Liu JJ, Liu YP, Jazag A, Guleng B, Ren JL. 2013. ECHS1 acts as a novel HBsAg-binding protein enhancing apoptosis through the mitochondrial pathway in HepG2 cells. Cancer Lett 330:67–73.

Zhang J, Lin A, Powers J, Lam MP, Lotz C, Liem D, Lau E, Wang D, Deng N, Korge P, Zong, NC, Cai H, et al. 2012. Perspectives on: SGP symposium on mitochondrial physiology and medicine: mitochondrial proteome design: from molecular identity to pathophysiological regulation. J Gen Physiol 139:395–406.

Mutations in *HADHB*, which Encodes the β-Subunit of Mitochondrial Trifunctional Protein, Cause Infantile Onset Hypoparathyroidism and Peripheral Polyneuropathy

Misako Naiki,[1,2] Nobuhiko Ochi,[3] Yusuke S. Kato,[4] Jamiyan Purevsuren,[5] Kenichiro Yamada,[1] Reiko Kimura,[1] Daisuke Fukushi,[1] Shinya Hara,[6] Yasukazu Yamada,[1] Toshiyuki Kumagai,[7] Seiji Yamaguchi,[5] and Nobuaki Wakamatsu[1]*

[1]Department of Genetics, Institute for Developmental Research, Aichi Human Service Center, Kasugai, Aichi, Japan

[2]Department of Pediatrics, Nagoya University Graduate School of Medicine, Nagoya, Aichi, Japan

[3]Department of Pediatrics, Daini-Aoitori Gakuen, Aichi Prefectural Hospital and Habilitation Center for Disabled Children, Okazaki, Aichi, Japan

[4]Institute for Health Science, Tokushima Bunri University, Tokushima, Japan

[5]Department of Pediatrics, Shimane University, Faculty of Medicine, Izumo, Shimane, Japan

[6]Department of Pediatrics, Toyota Memorial Hospital, Toyota, Aichi, Japan

[7]Department of Pediatric Neurology, Kobato Gakuen, Aichi Human Service Center, Kasugai, Aichi, Japan

Mitochondrial trifunctional protein (MTP) is a hetero-octamer composed of four α- and four β-subunits that catalyzes the final three steps of mitochondrial β-oxidation of long chain fatty acids. *HADHA* and *HADHB* encode the α-subunit and the β-subunit of MTP, respectively. To date, only two cases with MTP deficiency have been reported to be associated with hypoparathyroidism and peripheral polyneuropathy. Here, we report on two siblings with autosomal recessive infantile onset hypoparathyroidism, peripheral polyneuropathy, and rhabdomyolysis. Sequence analysis of *HADHA* and *HADHB* in both siblings shows that they were homozygous for a mutation in exon 14 of *HADHB* (c.1175C>T, [p.A392V]) and the parents were heterozygous for the mutation. Biochemical analysis revealed that the patients had MTP deficiency. Structural analysis indicated that the A392V mutation identified in this study and the N389D mutation previously reported to be associated with hypoparathyroidism are both located near the active site of MTP and affect the conformation of the β-subunit. Thus, the present patients are the second and third cases of MTP deficiency associated with missense *HADHB* mutation and infantile onset hypoparathyroidism. Since MTP deficiency is a treatable disease, MTP deficiency should be considered when patients have hypoparathyroidism as the initial presenting feature in infancy.
© 2014 Wiley Periodicals, Inc.

Key words: hypoparathyroidism; MTP deficiency; HADHB; LCKT; peripheral polyneuropathy

INTRODUCTION

MTP is a hetero-octamer composed of four α- and four β-subunits and contains three different enzyme activities that catalyze the final three chain-shortening reactions in the β-oxidation of long-chain fatty acids [Uchida et al., 1992]. *HADHA* encodes the α-subunit, which has both long-chain enoyl-CoA hydratase (LCEH, EC 4.2.1.17) and long-chain 3-hydroxyacyl-CoA dehydrogenase (LCHAD, EC 1.1.1.211) activities, whereas *HADHB* encodes the β-subunit, which has only long-chain 3-ketoacyl-CoA thiolase (LCKT, EC 2.3.1.16) activity [Uchida et al., 1992]. Mutations in *HADHA* or *HADHB* cause MTP (LCEH, LCHAD, LCKT) deficiency, with decreased activity and levels of all three enzymes because of the failure of hetero-octamer formation; however, a homozygous mutation (1528G>C) in *HADHA* has been reported to cause an isolated LCHAD deficiency [IJlst et al., 1994]. MTP deficiency is characterized by a wide range of clinical features, including cardiomyopathy, hypoketonic hypoglycemia, metabolic acidosis, sudden infant death, metabolic encephalopathy, liver dysfunction, peripheral neuropathy, exercise-induced myoglobinuria, and rhabdomyolysis [Wanders et al., 1999].

Hypoparathyroidism is a rare disorder characterized by hypocalcemia and hyperphosphatemia and is caused by deficiency in parathyroid hormone (PTH) action. An epidemiological survey showed that the prevalence of idiopathic hypoparathyroidism in Japan is 1:140,000 [Nakamura et al., 2000]. Impaired secretion of PTH causes PTH-deficient hypoparathyroidism, while resistance to PTH due to a defect in the PTH receptor or insensitivity to PTH results in pseudohypoparathyroidism. Autosomal recessive forms of isolated hypoparathyroidism have been reported to be caused by mutations in *PTH*, located on chromosome 11p15 [Parkinson and Thakker, 1992] or the gene encoding the parathyroid-specific transcription factor glial cells missing B (*GCMB*) on 6p24 [Ding et al., 2001].

Here, we report that two siblings born to consanguineous parents have MTP deficiency associated with infantile onset hypoparathyroidism. We have identified a new missense mutation in *HADHB* located close to the active site of the β-subunit of MTP. We also review hypoparathyroidism caused by MTP deficiencies and discuss the pathogenesis of the disease associated with hypoparathyroidism.

PATIENTS AND METHODS

Written informed consent was obtained from the patients and the family members who participated in this study. The experiments were conducted after approval by the institutional review board at the Institute for Developmental Research, Aichi Human Service Center.

The proband (IV-1) is an 18-year-old female born to first-cousin parents as a dizygotic twin (Fig. 1A). She was born at 37 weeks and 4 days gestation by normal vaginal delivery following an uneventful pregnancy. She was hospitalized 5 weeks after birth because of generalized seizures. Biochemical analysis revealed a decreased serum calcium concentration of 1.15 mmol/L (normal range: 2.25–2.75 mmol/L) and an elevated serum phosphorus concentration of 3.49 mmol/L (normal range: 1.21–2.18 mmol/L). The serum

concentration of intact-PTH (iPTH) was below detectable levels (<5 pg/ml; normal range: 10–65 pg/ml). The concentrations of serum creatinine and blood urea nitrogen (BUN) were 0.3 mg/dl (normal range: 0.1–0.4 mg/dl) and 7 mg/dl (normal range: 7–19 mg/dl), respectively; thus, renal function was normal. She was diagnosed with hypoparathyroidism and was treated with activated vitamin D and calcium. The therapy elevated the serum calcium concentration, and she no longer experienced seizures. At 1 year of age, her serum calcium concentration had increased to 2.00 mmol/L, but her serum iPTH concentration was undetectable (<5 pg/ml). She achieved all developmental milestones at the appropriate age. At 2 years, she was admitted to the hospital with tetany after an upper respiratory tract infection. Upon admission, laboratory examination revealed an elevated serum creatine kinase concentration of 9,577 U/L (normal range: 20–150 U/L) and a low serum calcium concentration of 1.48 mmol/L. She was diagnosed with rhabdomyolysis and hypocalcemia and was successfully treated with intravenous fluids. She was later admitted to the hospital with recurrent episodes of fever, hypocalcemia, rhabdomyolysis, and myoglobinuria for several years. She has also experienced distal lower limb muscle weakness and atrophy since 3 years of age. Because of having a drop foot, she has had difficulty walking and has used foot orthoses or a wheelchair since she was 9. A neurologic examination at 9 years of age demonstrated distal muscle weakness, particularly involving the peroneal muscles, with absent tendon reflexes. There were no signs of pyramidal tract involvement. The motor conduction velocity of the peroneal nerve was decreased to 21.6 m/sec (normal range: 40–65 m/sec). Sensory conduction velocity of the sural nerve could not be evoked. The Gower's sign was negative. Thus, she has peripheral sensorimotor polyneuropathy. A muscle biopsy from the left biceps brachii demonstrated denervation atrophy with a predominance of type I fibers. She currently presents with severe muscular atrophy of the lower legs and hands with an absence of Achilles and patellar tendon reflexes, which are the clinical features of Charcot-Marie-Tooth (CMT) disease. She also has a drop foot and hammer toes, and touch and vibration senses of the distal legs are diminished (Fig. 1B). The serum calcium and iPTH concentrations at present were 2.10 mmol/L and 5 pg/ml, respectively. Analysis of blood acylcarnitines and urine organic acids measured once in a non-acute phase showed no abnormalities.

Patient IV-2 is an 18-year-old male who is the dizygotic twin of Patient IV-1 (Fig. 1A). Because his twin sister had hypoparathyroidism at the age of 1 month, his serum concentration of iPTH was measured at 4 months. He was asymptomatic, but his serum iPTH concentration was undetectable (<5 pg/ml) with a decreased calcium concentration (1.50 mmol/L) and an elevated phosphorus concentration (3.97 mmol/L). He started a regimen of activated vitamin D and calcium. He did not experience seizures but developed progressive peripheral polyneuropathy, and has exhibited rhabdomyolysis triggered by fevers from viral infections since he was 3. At 9 years of age, the motor conduction velocity of the peroneal nerve was decreased to 35.6 m/sec, and sensory conduction velocity of the sural nerve was not evoked. Findings from a muscle biopsy performed at 10 years of age were similar to those obtained for his sister. At 10 years of age, he required ventilator support owing to respiratory failure following an episode of rhab-
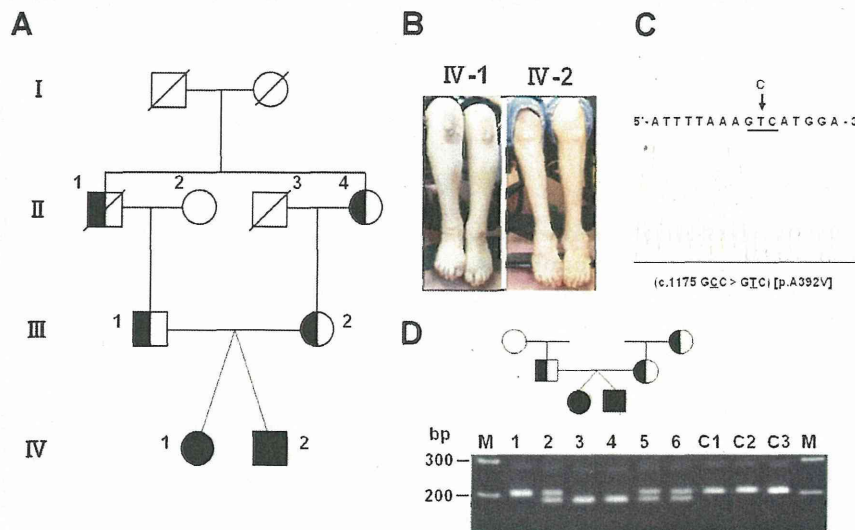
FIG. 1. The identification of the mutation in *HADHB*. A: The pedigree of the family with hypoparathyroidism and peripheral polyneuropathy. Affected individuals are indicated by filled symbols, unaffected individuals by unfilled symbols, and carrier individuals by half-filled symbols. B: The patients have muscle atrophy of the lower legs and deformity of the toes [hammer toes]. C: The direct sequence analysis of the patient IV-1 revealed a C to T substitution at nucleotide position 1175 in exon 14 of *HADHB*, resulting in the substitution of alanine [GCC] at codon 392 with valine [GTC] [c.1175C>T, [p.Ala392Val]], as indicated by the arrow. D: PCR-RFLP analysis using *Bsp*HI-digested PCR products from family members and three normal controls [C1, C2, and C3] were run through a 1.5% low-melting agarose gel. The sizes of the DNA markers are indicated on the left side.

domyolysis and myoglobinuria with a decreased calcium concentration (1.88 mmol/L) and a normal phosphorus concentration (1.93 mmol/L); however, his renal function was normal, as indicated by his serum creatinine (0.3 mg/dl) and BUN (17 mg/dl) concentrations. Analysis of blood acylcarnitines and urine organic acids in a non-acute phase showed no abnormalities. The serum calcium and iPTH concentrations at present were 2.20 mmol/L and 6 pg/ml, respectively. He currently presents with clinical features similar to those of his sister (Fig. 1B).

Patient IV-1 developed seizures due to hypoparathyroidism at 5 weeks after birth, and hypoparathyroidism was diagnosed in

Patient IV-2 at the age of 4 months. Thus, both patients presented with infantile onset hypoparathyroidism. The clinical features of the presented patients are summarized in Table I.

DNA Analysis

Genomic DNA was isolated from white blood cells by phenol/chloroform extraction. Specific primers were designed to amplify *PTH*, *GCMB*, *HADHA*, and *HADHB*. PCR-amplified DNA fragments were isolated, purified, and sequenced using the Big Dye Terminator Cycle Sequencing Kit (Applied Biosystems, Foster City,

TABLE I. Clinical and Molecular Features of Hypoparathyroidism Associated With MTP Deficiency

Patients	1	2	3	4
Gender	Female	Female	Female	Male
Age at onset				
Hypoparathyroidism	15 m	4 m	5 w	4 m
Rhabdomyolysis	15 m	15 m	2 y	3 y
Peripheral polyneuropathy	15 m	4 m	3 y	3 y
Hypotonia	+	+	−	−
Liver dysfunction	+	+	−	−
HADHA/HADHB mutation	ND	N389D (HADHB)	A392V (HADHB)	A392V (HADHB)
References	Dionisi-Vici et al. [1996]	Labarthe et al. [2006]	This study	This study

+, present; −, not present; ND, not described; w, week; m, month; y, year.

CA). Mismatch primer pairs (sense: 5'-tgctgggattacagatgtgag-3'; antisense: 5'-tgcaaaccaatcagaattcatg-3') were prepared for PCR-RFLP analysis to generate the *Bsp*HI site (tcatga) in a mutant allele. *Bsp*HI was used to digest the 200-bp mutant (c.1175C>T) PCR product, which generated the 178-bp PCR product.

Enzyme Assay

Mitochondrial LCKT activity in lymphoblastoid cells from the two patients and from two healthy adult males (as the control) was determined using 10 μM 2-ketopalmitoyl-CoA as a substrate [Purevsuren et al., 2009]. Citrate synthase activity was determined spectrophotometrically using DTNB.

MTP Expression Analysis

Cell extracts of lymphoblastoid cells from Patients IV-1 and IV-2 and two healthy adult males and of MTP-deficient fibroblasts (previously reported by Purevsuren et al. [2009]) were subjected to 12.5% sodium dodecyl sulfate-polyacrylamide gel electrophoresis (SDS-PAGE). Western blot analysis was performed using a rabbit polyclonal antibody specific for both the α- and β-subunits of MTP or medium-chain acyl-CoA dehydrogenase (MCAD) (both antibodies were generously provided by Dr. T. Hashimoto, Professor Emeritus, Shinshu University), and blots were visualized using the Immuno-Pure NBT/BCIP Substrate Kit (Promega, Madison, WI).

Construction of Wild-Type and Mutant HADHB-FLAG and Wild-Type HADHA-MYC Expression Vectors

The wild-type HADHB expression vector was prepared by subcloning *HADHB* cDNA at the *Not*I/*Eco*RV site of a mammalian expression vector, p3 × FLAG-CMV (Sigma–Aldrich, St. Louis, MO) (pHADHB-FLAG). An *Eco*RV recognition site (gatatc) was introduced at the termination codon (TAA) of *HADHB*. The mutant *HADHB* (pHADHB-A392V-FLAG, pHADHB-R61C-FLAG, pHADHB-N389D-FLAG, and pHADHB-R444K-FLAG; amino acid number is shown from the first methionine) and the wild-type *HADHA* (pHADHA-MYC) expression vectors were prepared using the in vitro mutagenesis method [Yamada et al., 2013]. The generated expression vectors encoded the FLAG-tagged wild-type or mutant β-subunits and MYC-tagged α-subunit protein at the *C*-terminus.

Analysis of the Association of the Wild-Type or Mutant β-Subunits With the Wild-Type α-Subunit

Various combinations of 0.4 μg of wild-type or mutant HADHB-FLAG expression vectors and 0.4 μg of the HADHA-MYC expression vector were co-transfected into HEK293 cells in 24-well dishes using Lipofectamine 2000 reagent (Life Technologies, Carlsbad, CA). Sixty hours after transfection, the cells were collected, and the extracts were subjected to immunoprecipitation using anti-FLAG

M2 antibody-conjugated agarose (Sigma–Aldrich) for 2 hr at 4°C with gentle mixing [Yamada et al., 2013]. After washing the gels, the precipitates were subjected to a 10% SDS-PAGE, and proteins were transferred to a PVDF membrane (Immobilon-P). Western blot analysis was performed with anti-FLAG M2 antibody (for the β-subunit) and with anti-MYC antibody (for the α-subunit, kindly provided by Dr. K. Nagata, Aichi Human Service Center). Immunoreactive bands were visualized with an enhanced chemiluminescence western blotting detection system (GE Healthcare, Waukesha, WI).

Structural Analysis of MTP

A homology model of human MTP was built using the Swiss-Model automated modeling server [Kiefer et al., 2009]. N389 and A392 of the β-subunit of the MTP coordinate (PDB code: 1wdk) [Ishikawa et al., 2004] were replaced with aspartate (D) and valine (V), respectively, using the Swiss PDB Viewer [Guex and Peitsch, 1997] to determine the effect of these substitutions on the surrounding residues.

RESULTS
Identification of the Mutation

The nucleotide sequences of all exons and splice sites of the candidate genes of autosomal recessive isolated hypoparathyroidism, *PTH* and *GCMB*, revealed no mutations. Since mutations of *HADHA* and *HADHB* cause rhabdomyolysis in infancy, we determined the nucleotide sequences of all exons and intron-exon boundaries of the genes from the patients and identified a homozygous mutation (c.1175C>T, [p.A392V]) in exon 14 of *HADHB* (NM_000183) (the first methionine is numbered as one) (Fig. 1C). PCR-RFLP analysis demonstrated that the patients were homozygous, whereas the parents and grandmother were heterozygous for the mutation (Fig. 1D). The mutation was absent in 200 normal alleles.

A392V in the β-Subunit Causes MTP Deficiency

The LCKT activities of the lymphoblastoid cells of the Patients IV-1 and IV-2 were decreased to 5% and 14% of normal controls, respectively (Fig. 2A). Western blot analysis showed faint or no bands for the α- and β-subunits bands of MTP from the patient's lymphoblastoid cells. In contrast, both subunits were clearly detected in control lymphoblastoid cells (Fig. 2B). Thus, the patients were found to have MTP deficiency caused by decreased amounts of α- and β-subunits.

The A392V β-Subunit Does Not Associate With the α-Subunit of MTP

Hetero-octamer formation of the four α- and four β-subunits is necessary for MTP activity. To confirm the MTP deficiency evaluated by the enzyme assay and western blot analysis, we studied the effect of mutant β-subunits on the formation of the MTP hetero-octamer with the α-subunit by immunoprecipitation. Western blot
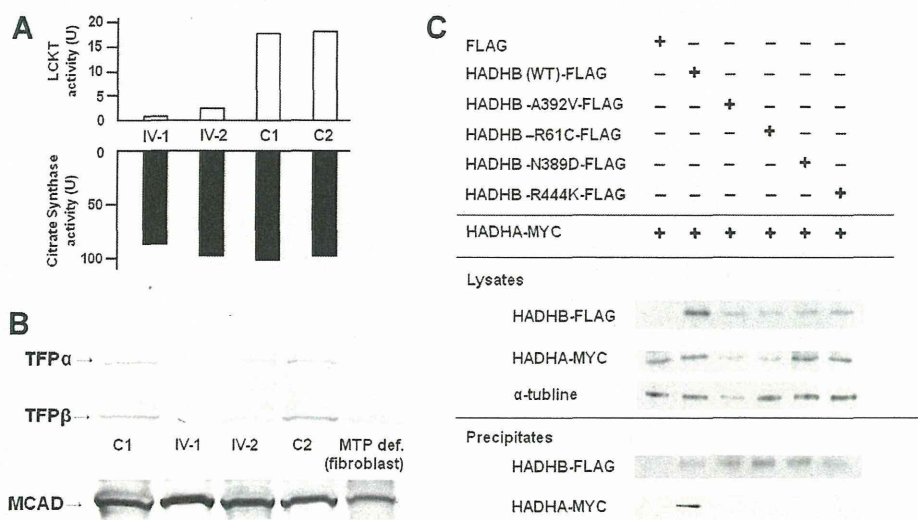
FIG. 2. Biochemical analyses of the MTP protein of the patients. A: The LCKT activities [upper panel] and citrate synthase activities [lower panel] in lymphoblastoid cells from the patients and two controls are shown [1U = μmol/min/mg protein]. B: Western blot analysis of the α- and β-subunits of MTP and MCAD protein [EC 1.3.99.3] [positive control] from the patients and controls lymphoblastoid cells and MTP-deficient fibroblasts are shown. C: Immunoprecipitation of the wild-type or mutant β-subunits with the wild-type α-subunit. [+] Indicates the FLAG- or MYC-tagged vectors used in each study. Lysates and precipitates were immunoblotted with antibodies as indicated [FLAG, MYC, and α-tubulin]. The results of western blot analysis are shown.

analysis revealed that expressions of the mutant β-subunit proteins were decreased in HEK293 cells (Fig. 2C, Lysates), but were efficiently precipitated (Fig. 2C, Precipitates). The MYC-tagged α-subunit co-precipitated with the FLAG-tagged wild-type β-subunit, whereas less than detectable levels of the α-subunit co-precipitated with the four mutant β-subunits (Fig. 2C). Thus, the A392V mutation, as well as the β-subunit N389D mutation previously reported as being associated with a hypoparathyroidism phenotype, abolished the formation of the MTP hetero-octamer, similar to other β-subunit mutations such as R61C (previously described as R28C; lethal phenotype) and R444K (previously described as R411K; neuromyopathic phenotype) [Spiekerkoetter et al., 2003; Purevsuren et al., 2009].

N389D and A392V Mutations Affect the Conformation of the β-Subunit

We analyzed a homology model of the β-subunit of human MTP. N389 and A392 of human MTP are located on the solvent-exposed surface of tetrameric MTP (Fig. 3A). These data indicated that N389 and A392 are not involved in the intersubunit interaction. The catalytic triad, composed of C138, H428, and C458 (shown as blue letters), is located very close to N389 and A392 in the homology model of human MTP (Fig. 3B). Moreover, N389 and A392 are both located on the Cα2 helix in the homology model and directly interact with the Cα1 helix. Notably, the hydrogen bond between the side chains of D389 and T356 is missing in the N389D human

MTP model (Fig. 3B,C), and a slight steric clash exists between the side chains of V392 and T356 in the A392V mutant model (Fig. 3D).

DISCUSSION

MTP deficiency caused by mutations of *HADHA* or *HADHB* has been classified into three clinical phenotypes: a lethal phenotype with neonatal onset (severe form), a hepatic phenotype with infantile onset (intermediate form), and a neuromyopathic phenotype with late-adolescent onset (mild form) [Spiekerkoetter et al., 2003]. The clinical features of the patients, together with their decreased LCKT activities, the decreased protein levels of both α- and β-subunits in the patients' lymphoblastoid cells, and the failure of the mutant β-subunit to form an active hetero-octamer with the wild-type α-subunit of the MTP protein indicate that the patients presented in this study have the neuromyopathic phenotype of MTP deficiency due to a homozygous A392V mutation in *HADHB*. Spiekerkoetter et al. [2004] reported that the neuromyopathic phenotype is the major phenotype of MTP deficiency. In contrast, only two of six Japanese cases reported in the literature have presented with the neuromyopathic phenotype [Purevsuren et al., 2009; Yagi et al., 2011]. The fact that the number of cases reported with the neuromyopathic phenotype in Japan is small is most likely because this phenotype is included in the differential diagnosis of early or late-adolescent onset CMT disease with or without episodic myoglobinuria [Spiekerkoetter et al., 2004].

Only two cases of MTP deficiency associated with hypoparathyroidism have been reported (Table I). Dionisi-Vici et al. [1996] first
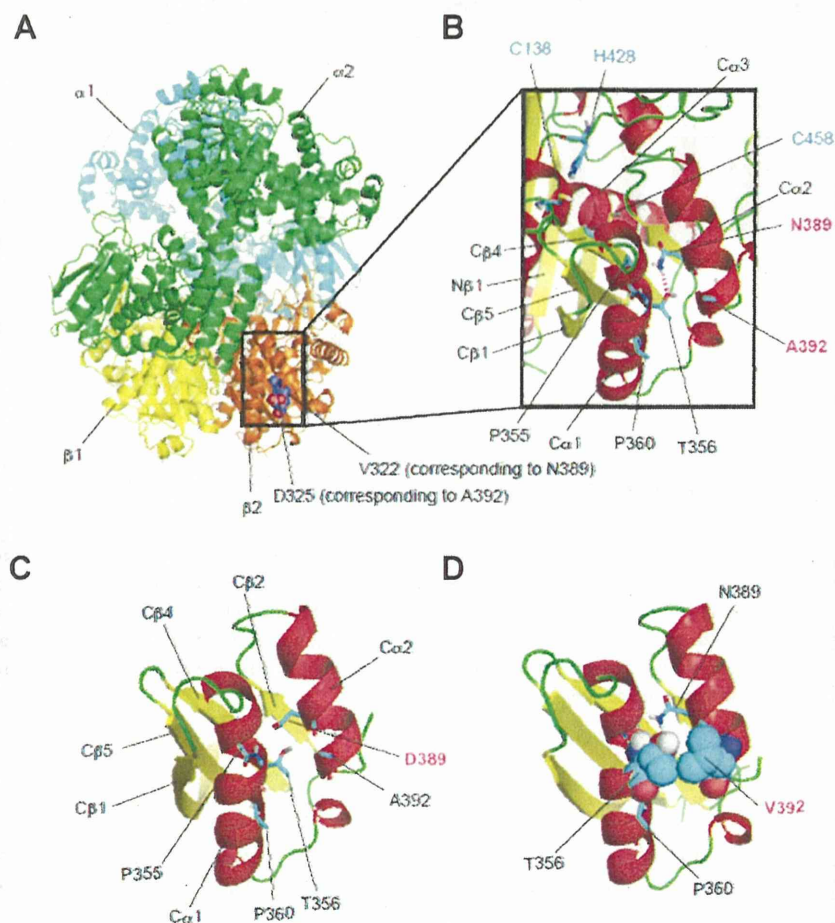
FIG. 3. Structure and homology modeling of MTP. A: α2β2 tetrameric structure of MTP. Molecules colored in cyan and green are the α-subunits [α1 and α2, respectively] of MTP from *Pseudomonas fragi*, whereas those colored in yellow and orange are the β-subunits [β1 and β2, respectively] [Ishikawa et al., 2004]. V322 and D325 are depicted as sphere models. These residues correspond to N389 and A392 of human MTP. B: Enlarged view of the homology model of one of the β-subunits of human MTP. α-helices and β-strands are colored in red and yellow, respectively. Hydrogen, carbon, oxygen, nitrogen, and sulfur atoms are colored in gray, cyan, red, blue, and yellow, respectively. Secondary structure nomenclature [Nβ1, Cβ1, Cβ4, Cβ5, Cα1, Cα2, and Cα3] defined in the yeast thiolase structure [Mathieu et al., 1997] is also indicated. Helices corresponding to Lα1 [171–175], Lα2, and Lα3 of yeast thiolase [V171-L260] have been removed for clarity. A hydrogen bond between the amino group of N389 and the hydroxyl group of T356 is depicted as a dotted line [pink]. C: View around the N389D mutation in the homology model of the β-subunit of human MTP. D: View around the A392V mutation. T356 and V392 are depicted as sphere models.

reported the case of a female patient with MTP deficiency and hypoparathyroidism. Hypoparathyroidism became apparent when she was admitted to the hospital because of fasting-induced rhabdomyolysis at 15 months of age. She had severe hypotonia, respiratory failure, and peripheral polyneuropathy without renal failure. Her serum iPTH concentration was low (4 pg/ml) with severe hypocalcemia (0.95 mmol/L), and the enzyme activities of MTP in the fibroblasts were all reduced: LCKT activity was absent, and LCHAD and LCEH activities were 30% and 52% of the control mean, respectively. These results indicate that she had MTP deficiency with a neuromyopathic phenotype, caused possibly by an *HADHB* mutation encoding LCKT. Labarthe et al. [2006] also reported a female case with hypoparathyroidism and MTP deficiency caused by a *HADHB* mutation. Hypo-

parathyroidism (iPTH <5 pg/ml) and severe hypocalcemia (1.2 mmol/L) became evident when she was 4 months old. A homozygous mutation (c.1165A>G, [p.N389D]) in *HADHB* was identified. Her serum iPTH concentration reached normal levels after vitamin D therapy, although she developed peripheral polyneuropathy with decreased nerve conduction velocity. LCKT activity was not reported, but numerous episodes of fasting-induced rhabdomyolysis suggested that she had a defective β-subunit of MTP. Indeed, we demonstrated that the N389D β-subunit does not associate with the wild-type α-subunit (Fig. 2C). Taken together, the sibling patients presented here and the two previously reported cases have similar clinical features of infantile onset hypoparathyroidism, peripheral polyneuropathy, and rhabdomyolysis.